

Label-Free Real-Time Monitoring of Reactions Between Internalin A and Its Antibody by an Oblique-Incidence Reflectivity-Difference Method

Xu Wang^{1*}, Galina Malovichko², Marcelo Mendonça³, Fabricio Rochedo Conceição³,
José AG Aleixo³, and Xiangdong Zhu²

¹Department of Fundamental Courses, Wuxi Institute of Technology, Wuxi 214121, P. R. China

²Department of Physics, University of California at Davis, Davis, CA 95616, USA

³Laboratório de Imunologia Aplicada, Núcleo de Biotecnologia, Centro de Desenvolvimento Tecnológico, Universidade Federal de Pelotas, Pelotas, RS 96010-900, Brazil

(Received August 24, 2015 : revised November 5, 2015 : accepted December 14, 2015)

Surface protein internalin (InIA) is a major virulence factor of the food-borne pathogen *L. monocytogenes*. It plays an important role in bacteria crossing the host's barrier by specific interaction with the cell adhesion molecule E-cadherin. Study of this protein will help to find better ways to prevent listeriosis. In this study, a monoclonal antibody against InIA was used to detect InIA. The reaction was label-free and monitored in real time with an oblique-incidence reflectivity-difference (OI-RD) technique. The kinetic constants k_{on} and k_{off} and the equilibrium dissociation constant K_d for this reaction were also obtained. These parameters indicate that the antibody is capable of detecting InIA. Additionally, the results also demonstrate the feasibility of using OI-RD for proteomics research and bacteria detection.

Keywords : Label-free, Reflectivity difference, Internalin

OCIS codes : (170.0110) Imaging systems; (240.2130) Ellipsometry and polarimetry; (240.6645) Surface differential reflectance

I. INTRODUCTION

L. monocytogenes is a human pathogen that causes listeriosis, a severe illness. Internalin A (InIA) is considered to be the most important surface protein of *L. monocytogenes*, because it promotes listeria uptake into intestinal epithelial cells by targeting the N-terminal domain of human E-cadherin, the dominant adhesion molecule of adherens junctions [1, 2]. Based on this fact, *L. monocytogenes* may cause illness in an intestinal, utero-placental, hepatic, or neurological phase of infection. Since the *L. monocytogenes* bacteria always hide in host cells, which makes it difficult for an antibiotic to work, a better way to prevent listeriosis is to block InIA from adhesion and invasion. Thus many researchers have turned their attention to InIA.

Most anti-listeria antibodies available from research laboratories or commercial vendors are associated with the problems of low affinity [3], reaction to heterologous antigens [4, 5], or lack of reaction toward all serotypes of *L. monocytogenes* [6, 7]. Recently, a group of researchers announced a

monoclonal antibody against InIA that reacts with both InIA and *L. monocytogenes* cells [8]. Known as Mab-2D12, it is reactive with all 13 serotypes of *L. monocytogenes*, but the affinity of this antibody to InIA has not been determined. To obtain information about the affinity of Mab-2D12, real-time measurements of the interaction between Mab-2D12 and InIA are desired. Further data analysis should provide the kinetic constants of the reaction.

A common way to obtain affinity information is by using a surface plasmon resonance (SPR) biosensor [9-12]. Recently an optical oblique-incidence reflectivity difference (OI-RD) method has also shown great potential in high-throughput proteomics research [13, 14]. The OI-RD method detects a biomolecular microarray by measuring thickness and mass density of target spots. A small change in thickness or mass density in a molecular layer leads to changes in reflectivity. OI-RD is compatible with all flat substrates, which makes surface modification in OI-RD more flexible [15].

In the present study, OI-RD was used for label-free,

*Corresponding author: wangxu@wxit.edu.cn

Color versions of one or more of the figures in this paper are available online.

real-time monitoring of the binding reaction of Mab-2D12 antibody with surface-bound InIA targets. We will show how the kinetic parameters are obtained from the observed binding curves.

II. EXPERIMENT

A typical setup for OI-RD from a microarray-covered solid surface is sketched in Fig. 1. The microscope uses a He-Ne laser ($\lambda = 633$ nm) for illumination. The complex differential reflectivity change $\Delta_p - \Delta_s$ across the microarray-covered surface is measured [14]. Here we define the OI-RD signal as $Im\{\Delta_p - \Delta_s\}$, which can be obtained directly from experiments. Since the average thickness d of a biomolecular microarray is much less than the optical wavelength λ , Zhu and coworker [16] have shown that

$$\begin{aligned} Im\{\Delta_p - \Delta_s\} &\cong \frac{\alpha(\epsilon_d - \epsilon_s)(\epsilon_d - \epsilon_0)}{\epsilon_d} \left(\frac{d}{\lambda}\right), \\ \alpha &= \frac{-4\pi(\tan\theta_{inc})^2 \cos\theta_{inc}}{\sqrt{\epsilon_0(\epsilon_s - \epsilon_0)(\epsilon_s/\epsilon_0 - (\tan\theta_{inc})^2)}}. \end{aligned} \quad (1)$$

Here θ_{inc} is the angle of incidence, and ϵ_0 , ϵ_d , and ϵ_s are respectively the optical dielectric constants of the surroundings, the molecular layer, and the substrate. When using OI-RD to monitor the immobilization of an antibody with surface-bound InIA targets, ϵ_d is the dielectric constant of the immobilized antibody, ϵ_0 is the dielectric constant of glass, and ϵ_s is the dielectric constant of the solutions in the flow cell.

Monoclonal antibody against InIA was raised in mice. Briefly, six-week-old female mice were administered intraperitoneally (i.p.) with approximately 1×10^8 cells/ml of heat-killed *L. monocytogenes* serotype 4b. Two weeks later, a mixture of heat-killed *L. monocytogenes* and $50 \mu\text{g}$

of rInIA prepared with incomplete Freund's adjuvant was administered i.p. every week for 8 weeks. The splenocytes were harvested from the mouse and fused with murine Sp2/O-Ag14 myeloma cells. Selected hybridoma clones were administered to pristine-primed mice to produce ascetic fluid for antibody production. Monoclonal antibody was purified by affinity chromatography using a protein A-Sepharose 4B column (GE Healthcare), and the class of the monoclonal antibody was determined by ELISA experiments [8].

The experimental procedure consisted of several steps. First, the 80-kDa InIA target was printed on the epoxy-functionalized glass slide by a GMS 417 pin-and-ring contact-printing robot arrayer (Genetic Microsystems) at a concentration of $8.75 \mu\text{M}$ in a solution of $1 \times \text{PBS}$ (phosphate buffered saline, pH = 7.4). Bovine serum albumin (BSA) was also printed as the control. InIA and BSA bind covalently to epoxy groups [17]. The arrangement of printed spots is shown in Fig. 2; the center-to-center separation between spots is $400 \mu\text{m}$. For each row, six spots were printed as repeats, and the slide was washed with $1 \times \text{PBS}$ solution to remove excess unbound and weakly bound proteins. Then the remaining epoxy groups on the surface were blocked with BSA ($7.6 \mu\text{M}$ in $1 \times \text{PBS}$) for 10 minutes, to prevent probe molecules from nonspecific binding. At last, the slide was reacted with Mab-2D12 antibody in $1 \times \text{PBS}$ at room temperature. We first filled the flow cell with antibody quickly at a rate of 30 mL/min, then slowed down the flow rate to 0.05 mL/min during observation of the association reaction. To observe the dissolution, we quickly replaced the probe solution with $1 \times \text{PBS}$ at a flow rate of 30 mL/min, then slowed down the flow rate to 0.05 mL/min during the subsequent dissociation.

III. RESULTS

In Figure 2 we show an OI-RD image of the InIA microarray at each step of the process. It is a small 4×6 microarray. The circles indicate where the spots should be, as printed. At the blocking and association step, it is unclear whether the reaction has happened by simply looking at Fig. 2, but from the difference image—the image after the association minus the image before—, it is clear that

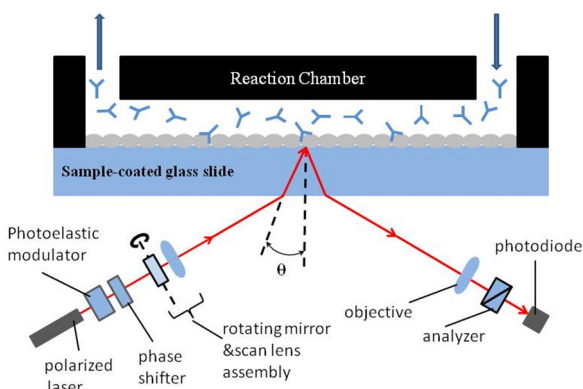


FIG. 1. Sketch of a scanning OI-RD for microarray detection. The microarray-bearing glass is mounted on a translation stage. The slide is also part of a flow cell.

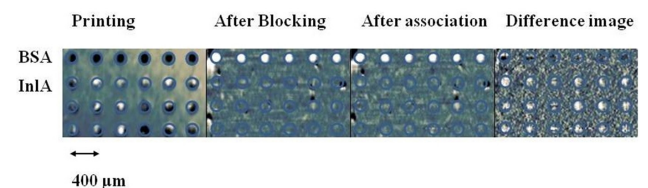


FIG. 2. OI-RD images of the microarray after printing, blocking, and association. The final difference image is obtained by subtracting the image after blocking from the image after association.

there were reactions between Mab-2D12 antibody and surface-bound InIA, while no reactions happened on the BSA spots. Here we rewrite Eq. (1) in terms of the surface mass density of the monolayer targets, given by $\Gamma_{probe} = d_{probe}\rho_{probe}$ [18],

$$\text{Im}\{\Delta_p - \Delta_s\} \cong \frac{\alpha(\epsilon_{probe} - \epsilon_s)(\epsilon_{probe} - \epsilon_0)}{\epsilon_{probe}} \left(\frac{\Gamma_{probe}}{\rho_{probe}\lambda} \right) \quad (2)$$

ϵ_{probe} is the dielectric constant for the antibody, ρ_{probe} is the volume mass density of the antibody, and d_{probe} is the average thickness of the immobilized antibody, which increases with time during association. Eq. (2) indicates that Γ_{probe} is proportional to $\text{Im}\{\Delta_p - \Delta_s\}$, which means the real-time OI-RD signal is proportional to the mass (quantity) of antibody molecules that have reacted with surface-bound InIA. The difference image in Fig. 2 shows positive signals at InIA spots, which proves that the reaction did take place.

Figure 3 shows three real-time binding curves with antibody at concentrations of 200 nM, 300 nM, and 400 nM: association in the first hour, and dissociation in the following two hours. Each curve is normalized to the maximum value of the OI-RD signal during association with antibody at 400 nM, assuming that a monolayer of antibody was immobilized on the surface after the association process. It is shown in Fig. 3 that the rates to reach saturation for the three curves are different. Saturation only occurred when the antibody was at a concentration of 400 nM. We fit the association-dissociation curves using Langmuir-reaction kinetics [19, 20]. In this model, the association rate is assumed to be proportional to the antibody concentration as $k_{on}[c]$, while the dissociation rate k_{off} is independent of the antibody concentration. The

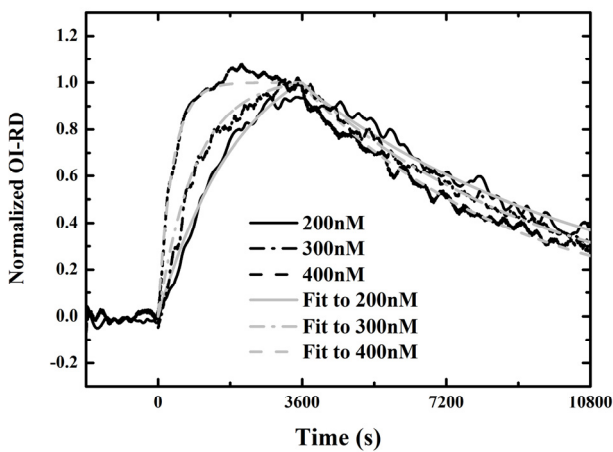


FIG. 3. Binding curves from InIA reacting with antibody at 200 nM (black solid line), 300 nM (black dash-dot line), and 400 nM (black dashed line). Association took place in the first hour, and dissociation followed in the later two hours. The gray traces are fits to the binding curves using a one-site Langmuir-reaction kinetic model.

equilibrium dissociation constant of the reaction is given by $K_d = k_{off}/k_{on}$. We fit the binding curves to a one-site Langmuir-reaction kinetic model that assumes one surface-bound InIA molecule reacts with one Mab-2D12 antibody molecule at a specific site.

In the one-site model, let N and $N^{(0)}$ be respectively the reacted and initially available amounts of antibody. The total amount of reacted antibody during the association reaction is given by

$$N(t) = \frac{N^{(0)}k_{on}[c]}{k_{on}[c] + k_{off}} (1 - \exp(-(k_{on}[c] + k_{off})t)) \quad (3)$$

Here $[c]$ is the concentration of antibody and t is time. After a time t_0 , the antibody solution is replaced with $1 \times$ PBS. Subsequently, the total number of the reacted antibody decreases as

$$N(t) = \frac{N^{(0)}k_{on}[c]}{k_{on}[c] + k_{off}} (1 - \exp(-(k_{on}[c] + k_{off})t_0)) \times \exp(-k_{off}(t - t_0)) \quad (4)$$

There is no doubt that the surface mass density Γ_{probe} is proportional to the amount of reacted antibody $N(t)$. From Eq. (2), the optical signals shown in Fig. 3 are expected to vary as

$$\text{Im}\{\Delta_p - \Delta_s\} \sim \frac{N^{(0)}k_{on}[c]}{k_{on}[c] + k_{off}} (1 - \exp(-(k_{on}[c] + k_{off})t)) \quad (5)$$

for $0 < t < t_0$, and

$$\text{Im}\{\Delta_p - \Delta_s\} \sim \frac{N^{(0)}k_{on}[c]}{k_{on}[c] + k_{off}} (1 - \exp(-(k_{on}[c] + k_{off})t_0)) \times \exp(-k_{off}(t - t_0)) \quad (6)$$

for $t > t_0$. For the three association-dissociation curves in Fig. 3, we performed a global fitting using Eqs. (5) and (6) with the same k_{on} and k_{off} as global fitting parameters. The three gray lines in the figure are the fits to the model. The kinetic constants for Mab-2D12 antibody reactions with InIA are $k_{on} = 3.35 \times 10^{-3} / (1/4 \mu\text{M} \cdot \text{s})$, $k_{off} = 1.14 \times 10^{-4} / \text{s}$, and $K_d = 3.40 \times 10^{-2} \mu\text{M} = 3.40 \times 10^{-8} \text{ M}$. The dissociation constant K_d obtained here falls within the range for biological molecules, from 1×10^{-4} to $1 \times 10^{-11} \text{ M}$ [21]. The data indicate that the monoclonal antibody is specific to the InIA protein. This experiment proves that the Mab-2D12 antibody is capable of detecting InIA protein and also whole-cell *L. monocytogenes*.

IV. CONCLUSION

In summary, we performed real-time, label-free monitoring of the reaction between Mab-2D12 antibody and surface-bound InIA. The appropriate dissociation constant $K_d = 3.40 \times 10^{-8}$ M indicates that Mab-2D12 antibody as a useful monoclonal antibody for the detection of *L. monocytogenes*. The results presented here also demonstrate the versatility of the combined OI-RD scanner and microarray platform for real-time monitoring of protein reaction kinetics, which confirms that OI-RD can be used to determine affinity of a protein with an antibody in a label-free manner.

ACKNOWLEDGMENT

This work was supported by the Natural Science Foundation of Jiangsu Higher Education Institutions of China (Grant No. BK20130116), the Fundamental Research Funds for the Central Universities of China (Grant No. JUSRP11011), the grants in the DocFix scholarship program (09/2012) of Marcelo Mendonça from FAPERGS - CAPES Brazil, and by US National Institutes of Health Grant Nos. RO1HG003827 and RO1HD065122.

REFERENCES

1. J. Mengaud, H. Ohayon, P. Gounon, R. Mege, and P. Cossart, "E-cadherin is the receptor for internalin, a surface protein required for entry of *L. monocytogenes* into epithelial cells," *Cell* **84**, 923-932 (1996).
2. C. D'Souza-Schorey, "Disassembling adherens junctions: breaking up is hard to do," *Trends Cell Biol.* **15**, 19-26 (2005).
3. A. K. Bhunia and M. G. Johnson, "Monoclonal antibody specific for *Listeria monocytogenes* associated with a 66-kilodalton cell surface antigen," *Appl. Environ. Microbiol.* **58**, 1924-1929 (1992).
4. A. K. Bhunia, P. H. Ball, A. T. Fuad, B. W. Kurz, J. W. Emerson, and M. G. Johnson, "Development and characterization of a monoclonal antibody specific for *Listeria monocytogenes* and *Listeria innocua*," *Infect. Immun.* **59**, 3176-3184 (1991).
5. S. H. Kim, M. K. Park, J. Y. Kim, P. D. Chuong, Y. S. Lee, B. S. Yoon, K. K. Hwang, and Y. K. Lim, "Development of a sandwich ELISA for the detection of *Listeria* spp. using specific flagella antibodies," *J. Vet. Sci.* **6**, 41-46 (2005).
6. S. A. Heo, R. Nannapaneni, R. P. Story, and M. G. Johnson, "Characterization of new hybridoma clones producing monoclonal antibodies reactive against both live and heat-killed *Listeria monocytogenes*," *J. Food Sci.* **72**, M008-M015 (2007).
7. M. Lin, S. Armstrong, J. Ronholm, H. Dan, M. E. Auclair, Z. Zhang, and X. Cao, "Screening and characterization of monoclonal antibodies to the surface antigens of *Listeria monocytogenes* serotype 4b," *J. Appl. Microbiol.* **106**, 1705-1714 (2009).
8. M. Mendonça, N. L. Conrad, F. R. Conceição, A. N. Moreira, W. P. Silva, J. A. Aleixo, and A. K. Bhunia, "Highly specific fiber optic immunosensor coupled with immunomagnetic separation for detection of low levels of *Listeria monocytogenes* and *L. ivanovii*," *BMC Microbiol.* **12**, 275 (2012).
9. H. Joung, W. Shim, D. Chung, J. Ahn, B. H. Chung, H. Choi, S. Ha, K. Kim, K. Lee, C. Kim, K. Kim, and M. Kim, "Screening of a specific monoclonal antibody against and detection of *Listeria monocytogenes* whole cells using a surface plasmon resonance biosensor," *Biotechnol. Bioprocess Eng.* **12**, 80-85 (2007).
10. K. M. Byun, "Development of nanostructured plasmonic substrates for enhanced optical biosensing," *J. Opt. Soc. Korea* **14**, 65-76 (2010).
11. B. P. Nelson, T. E. Grimsrud, M. R. Liles, R. M. Goodman, and R. M. Corn, "Surface plasmon resonance imaging measurements of DNA and RNA hybridization adsorption onto DNA microarrays," *Anal. Chem.* **73**, 1-7 (2001).
12. F. Yu, D. Yao, and W. Knoll, "Surface plasmon field-enhanced fluorescence spectroscopy studies of the interaction between an antibody and its surface-coupled antigen," *Anal. Chem.* **75**, 2610-2617 (2003).
13. J. P. Landry, Y. Y. Fei, and X. D. Zhu, "Simultaneous measurement of 10,000 protein-ligand affinity constants using microarray-based kinetic constant assays," *Assay Drug Dev. Technol.* **10**, 250-259 (2012).
14. J. P. Landry, Y. Y. Fei, and X. D. Zhu, "High throughput, label-free screening small molecule compound libraries for protein-ligands using combination of small molecule microarrays and a special ellipsometry-based optical scanner," *Int. Drug Discov.* **6**, 8-13 (2012).
15. R. Sandipan, M. Gunjan, and S. Sanjeeva, "Label-free detection techniques for protein microarrays: Prospects, merits and challenges," *Proteomics* **10**, 731-748 (2010).
16. X. D. Zhu, "Oblique-incidence optical reflectivity difference from a rough film of crystalline material," *Phys. Rev. B* **69**, 115407 (2004).
17. B. A. Rozenberg, "Kinetics, thermodynamics and mechanism of reactions of epoxy oligomers with amines," *Epoxy Resins and Composites II Advances in Polymer Sciences* **75**, 113-165 (1986).
18. J. A. De Feijter, J. Benjamins, and F. A. Veer, "Ellipsometry as a tool to study the adsorption behavior of synthetic and biopolymers at the air-water interface," *Biopolymers* **17**, 1759-1772 (1978).
19. I. Langmuir, "The constitution and fundamental properties of solids and liquids," *J. Am. Chem. Soc.* **38**, 2221-2295 (1916).
20. K. House-Pompeo, J. O. Boles, and M. Höök, "Characterization of bacterial adhesin interactions with extracellular matrix components utilizing biosensor technology," *METHODS: A Companion to Meth. Enz.* **6**, 134-142 (1994).
21. M. J. Pazos, A. Alfonso, M. R. Vieytes, T. Yasumoto, J. M. Vieites, and L. M. Botana, "Resonant mirror biosensor detection method based on yessotoxin-phosphodiesterase interactions," *Anal. Biochem.* **335**, 112-118 (2004).

CONTENTS

Regular Papers

- 1 Propagation Properties of a Partially Coherent Flat-Topped Vortex Hollow Beam in Turbulent Atmosphere
| *Dajun Liu, Yaochuan Wang, Guiqiu Wang, and Hongming Yin*
- 8 Ghost Imaging with Different Speckle Sizes of Thermal Light
| *Jue Wang, Renlong Yu, Yu Xin, Yanming Shao, Yanru Chen, and Qi Zhao*
- 13 Hybrid Atmospheric Compensation in Free-Space Optical Communication
| *Tingting Wang and Xiaohui Zhao*
- 22 Study of an Optical Goniometer Using a Multi-Photodiode Sensor
| *Ji-Sun Kim, A-Hee Kim, Han-Byeol Oh, Jun-Sik Kim, Bong-Jun Goh, Eun-Suk Lee, Ju-Hyeon Choi, Jin-Young Baek, and Jae-Hoon Jun*
- 29 Convex Optimization Approach to Multi-Level Modulation for Dimmable Visible Light Communications under LED Efficiency Droop
| *Sang Hyun Lee, Il-Kyu Park, and Jae Kyun Kwon*
- 36 Conflict Graph-based Downlink Resource Allocation and Scheduling for Indoor Visible Light Communications
| *Huanlin Liu, Hongyue Dai, Yong Chen, and Peijie Xia*
- 42 Hybrid Color and Grayscale Images Encryption Scheme Based on Quaternion Hartley Transform and Logistic Map in Gyration Domain
| *Jianzhong Li*
- 55 Asymmetric Public Key Cryptography by Using Logic-based Optical Processing
| *Sang Keun Gil*
- 64 A Compact Top-View Conformal Optical System Based on a Single Rotating Cylindrical Lens with Wide Field of Regard
| *Linyao Yu, Qun Wei, Jinggao Zheng, Mingda Ge, and Tianyi Zhang*
- 70 Quality Enhancement of a Complex Holographic Display Using a Single Spatial Light Modulator and a Circular Grating
| *Le Thanh Bang, Yun-Ling Piao, Jong-Jae Kim, and Nam Kim*
- 78 Role of Arbitrary Intensity Profile Laser Beam in Trapping of RBC for Phase-imaging
| *Ranjeet Kumar, Vishal Srivastava, Dalip Singh Mehta, and Chandra Shakher*
- 88 Laser Speckle Contrast Imaging for Measuring Cerebral Blood Flow Changes Caused by Electrical Sensory Stimulation
| *Ahna Cho, Chanmi Yeon, Donghyeon Kim, and Eunheon Chung*
- 94 A Coaxial and Off-axial Integrated Three-mirror Optical System with High Resolution and Large Field of View
| *Zhe Chen, Junqing Zhu, Jiantao Peng, Xingxiang Zhang, and Jianyue Ren*
- 101 Phase Only Pupil Filter Design Using Zernike Polynomials
| *Jiang Liu, Erlong Miao, Yongxin Sui, and Huaijiang Yang*
- 107 Three Degrees of Freedom Global Calibration Method for Measurement Systems with Binocular Vision
| *Guan Xu, Xinyuan Zhang, Xiaotao Li, Jian Su, Xue Lu, Huaping Liu, and Zhaobing Hao*
- 118 Optimization of Cutoff Shields in Projection Headlight Systems to Achieve High Intensity Gradient and Low Color Separation at the Cutoff Line
| *Byung-Yun Joo and Jae-Hyeon Ko*
- 125 Investigation on HT-AlN Nucleation Layers and AlGaN Epifilms Inserting LT-AlN Nucleation Layer on C-Plane Sapphire Substrate
| *Dang-Hui Wang and Tian-Han Xu*
- 130 The Influence of Rapid Thermal Annealing Processed Metal-Semiconductor Contact on Plasmonic Waveguide Under Electrical Pumping
| *Yang Lu, Hui Zhang, and Ting Mei*
- 135 Vector Passive Harmonic Mode-locking Fiber Laser Based on Topological Insulator Bi₂Se₃ Interacting with Fiber Taper
| *Jian Ping Li*
- 140 Distortion Correction Modeling Method for Zoom Lens Cameras with Bundle Adjustment
| *Wei Fang and Lianyu Zheng*
- 150 Performance Evaluation of MTF Peak Detection Methods by a Statistical Analysis for Phone Camera Modules
| *Jong-Hoon Kwon, Hyug-Gyo Rhee, Young-Sik Ghim, and Yun-Woo Lee*
- 156 Poincare Sphere Analysis of the Pretilt Angle Effect on the Viewing Angle of a Single-Domain FFS Liquid-Crystal Mode
| *Dong-Jun Lee, Seong-Woo Oh, Gyu-yeop Shim, Jun-Chan Choi, Joun-Ho Lee, Byeong Koo Kim, and Hak-Rin Kim*
- 165 Label-Free Real-Time Monitoring of Reactions Between Internalin A and Its Antibody by an Oblique-Incidence Reflectivity-Difference Method
| *Xu Wang, Galina Malovichko, Marcelo Mendonca, Fabricio Rochedo Conceicao, Jose AG Aleixo, and Xiangdong Zhu*
- 169 Investigation on Terahertz Generation by GaP Ridge Waveguide Based on Cascaded Difference Frequency Generation
| *Zhongyang Li, Kai Zhong, Pibin Bing, Sheng Yuan, Degang Xu, and Jianquan Yao*
- 174 A New Full-Aperture Reflective Null Measuring Method for Conformal Dome
| *Xudong Yan, Junhua Wang, and Min Xu*
- 180 Independent Color Filtering of Differently Polarized Light Using Metal-Insulator-Metal Type Guided Mode Resonance Structure
| *Young Jin Jung and Namkyoo Park*
- 188 Dependence of Q Factor on Surface Roughness in a Plasmonic Cavity
| *Yoon-Ho Kim, Soon-Hong Kwon, Ho-Seok Ee, Yongsop Hwang, You-Shin No, and Hong-Gyu Park*
- 192 Distributions of Amplitude and Phase Around C-points: Lemon, Mon-Star, and Star
| *Renlong Yu, Dong Ye, Yu Xin, Yanru Chen, and Qi Zhao*
- 199 Prediction of Glucose Concentration in a Glucose-Lactose Mixture Based on the Reflective Optical Power at Dual Probe Wavelengths
| *Song Gao, Wenjing Yue, and Sang-Shin Lee*
- 204 Identification and Determination of Oil Pollutants Based on 3-D Fluorescence Spectrum Combined with Self-weighted Alternating Trilinear Decomposition Algorithm
| *Pengfei Cheng, Yutian Wang, Zhikun Chen, and Zhe Yang*
- 212 Manuscript Submission Form
- 213 Copyright Transfer Agreement
- 214 Information for Contributors
- 215 The Journal of the Optical Society of Korea (JOSK) Paper Submission Regulations
- 218 Research Ethics of the Optical Society of Korea

Journal of the Optical Society of Korea

Vol. 20 No. 1

February 2016

Journal of the Optical Society of Korea

February 2016
VOLUME 20/ NUMBER 1

01